

Parity Violating Electron Scattering in the Resonance Region (Res-Parity)

June 27, 2005

P. E. Bosted<sup>1</sup> (spokesperson), E. Chudakov, V. Dharmawardane (co-spokesperson),

A. Deur, R. Ent, D. Gaskell, J. Gomez, X. Jiang, M. Jones,

R. Michaels, B. Reitz, J. Roche, B. Wojtsekhowski

*Jefferson Lab, Newport News, VA 23606*

J. Arrington (co-spokesperson), K. Hafidi, R. Holt, H. Jackson

D. Potterveld, P.E. Reimer, X. Zheng (co-spokesperson)

*Argonne National Lab, Argonne, IL 60439*

W. Boeglin, P. Markowitz

*Florida International University, Miami, FL 33199*

C. Keppel

*Hampton University, Hampton, VA 23668*

E. Hungerford

*University of Houston, Houston, TX*

G. Niculescu, I. Niculescu

*James Madison University, Harrisonburg, VA 22807*

T. Forest, N. Simicevic, S. Wells

*Louisiana Tech University, Ruston, LO 71272*

E. J. Beise, F. Benmokhtar

*University of Maryland, College Park, MD 20742*

K. Kumar, K. Paschke

*University of Massachusetts, Amherst, MA 01003*

F. R. Wesselmann

*Norfolk State University, Norfolk, VA*

Y. Liang, A. Opper

*Ohio University, Athens, Ohio 45701*

P. Decowski

*Smith College, Northampton, MA 01063*

R. Holmes, P. Souder

*University of Syracuse, Syracuse, NY 13244*

S. Connell, M. Dalton

*University of Witwatersrand, Johannesburg, South Africa*

R. Asaturyan, H. Mkrtchyan (co-spokesperson), T. Navasardyan, V. Tadevosyan

---

<sup>1</sup>Email: bosted@jlab.org

**Abstract**

We propose to perform the first measurements of the parity violation (PV) asymmetries  $A_p$ ,  $A_d$ , and  $A_C$  over the full resonance region ( $1 < W < 2.1$  GeV) at  $Q^2 \approx 0.8$  GeV<sup>2</sup>. The measurements consist of scattering 4.8 GeV longitudinally polarized electrons from unpolarized hydrogen, deuterium, and carbon targets at a scattering angle centered on 12.5 degrees, using the HRS-L and HRS-R spectrometers in Hall A. The projected total asymmetry errors are approximately 5% (relative) in each of four regions in  $W$ . The overall error is projected to be about 3% for each target (equal statistical and systematic errors), and the error on the ratios  $A_p/A_d$  and  $A_C/A_d$  is projected to be about 4% (dominated by statistical errors).

The goals include the study of resonance structure in  $A_p$  and  $A_d$ , and exploring both global and local quark-hadron duality with the previously un-studied combination of structure functions probed by PV inelastic electron scattering. The carbon target allows an investigation of the EMC effect that emphasizes the d quark contributions. The PV asymmetry is particularly sensitive to the isospin decomposition, as well as the axial hadronic current. The results are of great practical importance in more accurately modeling neutrino interactions in the few GeV region, which is essential in the interpretation of neutrino oscillation experiments. The new data are needed for modeling of radiative corrections to PV in the DIS region, and will also help in understanding backgrounds for other PV experiments.

The experiment will use the same Compton polarimeter, targets, detectors, and electronics as the planned experiment E05-007 (DIS-parity). The use of a lower beam energy (4.8 GeV compared to 6 GeV) is the only essential difference. We request a total of 14 days of production running and 1 day of checkout and calibrations.

## Contents

<b>1</b>	<b>Introduction and Motivation</b>	<b>3</b>
<b>2</b>	<b>Physics</b>	<b>6</b>
2.1	Parity Violating Asymmetry . . . . .	6
2.2	Resonance Region Asymmetry . . . . .	7
2.3	Deep-Inelastic Asymmetry . . . . .	8
2.4	Duality . . . . .	10
<b>3</b>	<b>Experiment</b>	<b>13</b>
3.1	Optimization of Kinematics . . . . .	14
3.2	Beam Line and Polarimetry . . . . .	14
3.3	Parity DAQ (Hall A) . . . . .	15
3.4	The Liquid Target . . . . .	15
3.5	Luminosity Monitor . . . . .	15

3.6	Spectrometers and Pole-tip Background . . . . .	16
3.7	Particle Identification Detectors . . . . .	16
3.8	Fast Counting DAQ . . . . .	17
3.8.1	FADC-based DAQ . . . . .	17
3.8.2	Scaler-based DAQ . . . . .	19
<b>4</b>	<b>Expected Results</b>	<b>20</b>
4.1	Kinematic Coverage . . . . .	20
4.2	Statistical and Systematic Uncertainties . . . . .	20
4.3	Beam Polarization . . . . .	22
4.4	Kinematic determination of $Q^2$ . . . . .	22
4.5	Electromagnetic Radiative Corrections . . . . .	23
4.6	Electroweak Radiative Corrections . . . . .	24
4.7	Beam Asymmetries . . . . .	24
4.8	Pion Contamination . . . . .	24
4.9	Pair Symmetric Background . . . . .	25
4.10	Target Related Systematics . . . . .	25
<b>5</b>	<b>Request</b>	<b>25</b>
<b>6</b>	<b>Physics Summary</b>	<b>26</b>
<b>7</b>	<b>Collaboration</b>	<b>27</b>

## 1 Introduction and Motivation

The electromagnetic interaction has proved very successful in probing the structure of the nucleon. Inelastic electron scattering at high momentum transfer  $Q^2$  and excitation energy  $\nu$  (corresponding to large missing mass  $W$ ) has provided the best information to date on the parton distribution functions, whose universal nature makes them useful in understanding a wide variety of particle interactions with nucleons. One limitation is that spin-averaged inclusive electron scattering probes quarks weighted by their charge squared: for a proton target this means that the contribution from down and strange quarks is strongly suppressed relative to the up quarks. Our best information on the down quark PDFs come from using a neutron target, although at high momentum fraction  $x = Q^2/2M\nu$  (where  $M$  is the nucleon mass), corrections from nuclear binding (Fermi motion) become large. Because the weak charges of the strange and down quarks are relatively larger than the electromagnetic ones, the weak interaction can provide another sensitive means to probe the down and strange PDFs.

An alternative basis for the description of nucleon excitations is in terms of transition form factors to specific resonant states. Lately, the subject of quark-hadron duality has received considerable interest, both theoretically and experimentally. Theoretical interest comes about in making a unified QCD description of the hadronic interactions.

Experimental interest arises because to the extent that duality works, it can be used to extract both spin-averaged and spin-dependent PDFs at large  $x$ . Duality is also of great importance experimentally to predict cross sections in regions where they haven't been measured precisely (for example, in predicting neutrino scattering cross sections needed to interpret neutrino oscillation experiments). The weak neutral current gives access to the axial hadronic current, which also enters in weak charge current interactions.

Electron scattering measurements sensitive to the weak neutral current are quite limited. The pioneering experiment of Prescott *et al.* [1] using inelastic scattering on the deuteron helped establish the standard electroweak model. The relatively large errors on the parity-violating asymmetry  $A_d$  measured in this experiment are no longer relevant in constraining physics beyond the Standard Model, or in constraining the strange quark PDFs. The experimental program at HERA at very high  $Q^2$  (comparable to  $M_Z^2$ , where  $M_Z$  is the  $Z$ -boson mass) are of limited statistical precision. Most electron PV experiments have focused on elastic channels, with the goal of probing the strange quark form factor of the nucleon (SAMPLE at Bates, HAPPEX and G0 at JLab, A4 at Mainz, etc.), and ultimately searching for physics beyond the standard Model (QWeak and DIS-parity at JLab). The G0 collaboration plans to study the  $N - \Delta$  transition at large electron scattering angles and DIS-parity (E05-007) was approved by the previous PAC to make a phase I measurement in the DIS region at 6 GeV ( $Q^2=1.1$  GeV<sup>2</sup>,  $W^2=4.2$  GeV<sup>2</sup> and  $Q^2=1.9$  GeV<sup>2</sup>,  $W^2=5.3$  GeV<sup>2</sup>), but there are presently no approved experiments to extend PV inelastic electron scattering into the full resonance region ( $W < 2.1$  GeV). With an 11 GeV electron beam at JLab, or a 30 GeV beam at SLAC, it will be possible to repeat the original Prescott experiment with more than an order-of-magnitude reduction in error bars. This will allow a competitive search for new physics, or to establish coupling of new particles if they have already been found at LHC. One hint that such new physics may exist comes from the observation of a 3-sigma discrepancy with the Standard Model from the NuTeV neutrino scattering experiment at Fermilab [2]. However, conventional explanations of this discrepancy also exist, for example a particle-antiparticle asymmetry in the strange sea, charge symmetry violation, or higher twist corrections.

The interpretation of a new high-precision electron scattering experiment will rely on a reasonable understanding of scattering at lower energy and  $W$ , through radiative effects. If a given experiment measures electron scattering with incident energy  $E_0$  and scattered electron energy  $E'_0$ , the helicity-dependent cross sections must be known at all energies  $E > E'_0$  and all  $E'_0 < E' < E_0$ . For  $E_0 = 11$  GeV,  $E'_0$  will typically be 3 to 5 GeV (see JLab 12 GeV pCDR), so measurements are needed down to  $E = 3$  GeV. This data will also allow for improved radiative corrections for the 6 GeV DIS-parity measurement.

Lower energy data will also be crucial to understand the role of higher twist corrections, which are generally expected to decrease with powers of  $Q^2$  and/or  $W^2$ . Measurements over a large range of  $Q^2$  and  $W$  are needed to measure higher twist diagrams, because there are no models to calculate them reliably.

Another motivation for this proposal comes from the desire to understand backgrounds in other PV experiments. In the recently completed E158 experiment [4] at

SLAC, the primary electron-electron (Møller) scattering signal was mixed with electron-proton scattering background, enhanced through radiative effects by the relatively long 180 cm LH2 target. While the  $ep$  elastic contributions are relatively well understood, the inelastic contribution (with an asymmetry about 20 times larger than the Møller asymmetry), turned out to generate the largest correction to the measured asymmetry and yields the largest systematic error of this experiment (22 ppb, or 17% relative). While measurements were made in a special detector that measured only  $ep$  scattering, the  $W$ -range was quite different than that of the Møller detectors, and elastic and inelastic contributions were strongly mixed. Dedicated measurements of the  $W$  dependence of PV inelastic scattering will help to build confidence in the systematic error on the E158 result, which is at present one of the three most precise Standard Model tests away from the Z-pole, and will also be of value for future Møller PV experiments, for example with JLab at 12 GeV.

The study of the resonance region is also of interest in its own right. In the quark-hadron duality picture, the response averaged over resonances should equal that at higher  $Q^2$ , once target mass corrections and leading-log effects are taken into account [5, 6, 7, 8, 9]. Because of the much different isospin structure and different couplings, the weak current will couple to individual resonances differently than the electromagnetic current, which can help in identifying new or poorly established resonances. We already have an indication that duality in the weak neutral current will work at the 20% to 30% level in a leading order valence picture of the vector hadronic current, as discussed in more detail below. What is of interest is to study the deviations due to the different mixture of resonances, their isospin structure, and their axial form factors. Since no measurements exist at present, it is not impossible that surprises await, and deviations from the leading order picture could be even larger than 30%.

A better understanding of the weak interaction at low  $Q^2$  (1 to 3 GeV<sup>2</sup>) is of great importance in understanding low energy neutrino interactions, which in turn are needed to determine neutrino masses and couplings through neutrino oscillation experiments [10, 11]. Neutrino oscillations in the channel  $\nu_\mu \rightarrow \nu_\tau$  will be studied by  $\tau$  production from neutrinos at underground neutrino telescopes like AMANDA, ANTARES, BAIKAL, and NESTOR, and with long base-line accelerator experiments like ICARUS, MINOS, MINER $\nu$ A, MONOLITH, and OPERA. Future high-accuracy experiments such as NO $\nu$ A and T2K will require even better knowledge of neutrino cross sections. In most experiments, the neutrinos have sufficient energy so that the excitation of nucleon resonances is possible. To go from the  $\tau$  yield to incident neutrino flux, one needs accurate predictions for the cross section integrated over the neutrino energy spectrum. This involves the three charged current structure functions  $W_1$ ,  $W_2$ , and  $W_3$ . Using isospin symmetry,  $W_1$  and  $W_2$  can be related to measurements using inclusive unpolarized electron scattering, and essentially depend on a knowledge of the hadronic vector current. PV electron scattering places additional constraints on the structure functions because of the very different weighting of isoscalar and isovector amplitudes compared to unpolarized scattering. Spin-averaged scattering is highly dominated by the  $u$  quarks, while PV scattering has relatively strong  $d$  quark contributions. Also, PV scattering is some-

what sensitive to the axial nucleon current. Modeling of neutrino cross sections requires assumptions such as PCAC to relate vector and axial current that may break down with increasing energy, so experimental constraints from PV scattering are useful [11]. The role of duality in the weak current has been discussed and the literature [12], and can be tested with the present proposal.

Isospin separation with unpolarized electrons relies on the use of neutrons embedded in nuclei such as deuterium, in which the effects of Fermi motion and Pauli suppression must be taken into account. On the other hand PV electron scattering on the proton allows access to a new isospin combination free from these effects. Since most neutrino experiments use nuclear targets, it is especially important to understand how the EMC effect changes the effective  $u$  and  $d$  quark distributions individually (or equivalently the isospin decomposition of the nucleon resonances). Unpolarized electron scattering is dominated by the effective  $u$  quark distributions at high  $x$ , while PV electron scattering has a large sensitivity to the effective  $d$  quark distributions. This makes PV electron scattering data a new way to help separate the EMC effect in valence and sea quarks [13]. While this data is largely in the resonance region, this is the precisely the region that dominates interactions in many of the high precision neutrino measurements. In addition, nuclear dependence of the  $F_2$  structure function shows identical behavior in the DIS and resonance region, down to very low  $W^2$  values [14]. Recent work showing a very different EMC effect for spin structure functions [15, 16], with a noticeable difference in the effect on the up and down quark distributions [15], makes such a measurement all the more appealing.

Our proposed measurements at the 5% level for about eight values of  $W$  from threshold through the resonance region and slightly into the DIS region ( $W = 2.1$  GeV) should be useful in building confidence in the models used to predict the neutrino cross sections, and complement the direct measurements planned at MINER $\nu$ A [10].

All of these observations suggest that it is long overdue to measure the PV asymmetry  $A_p$ ,  $A_d$ , and  $A_C$  in inelastic electron scattering at low  $Q^2$ . JLab is the only laboratory with sufficient beam energy and intensity to make these measurements in a meaningful way.

## 2 Physics

### 2.1 Parity Violating Asymmetry

Figure 1 shows the lowest-order Feynman diagrams for inelastic lepton-nucleon scattering for electromagnetic and weak interactions. Electrons can scatter off of protons by exchanging either a virtual photon,  $\gamma^*$ , or a  $Z^0$ . Therefore the cross section for lepton-nucleon scattering can be written as,

$$d\sigma = d\sigma_\gamma + d\sigma_{weak} + d\sigma_I, \quad (1)$$

where  $d\sigma_\gamma$  is the electromagnetic,  $d\sigma_{weak}$  is the weak and  $d\sigma_I$  is the interference contributions to the total cross section. For low-energy small-momentum-transfer lepton-nucleon

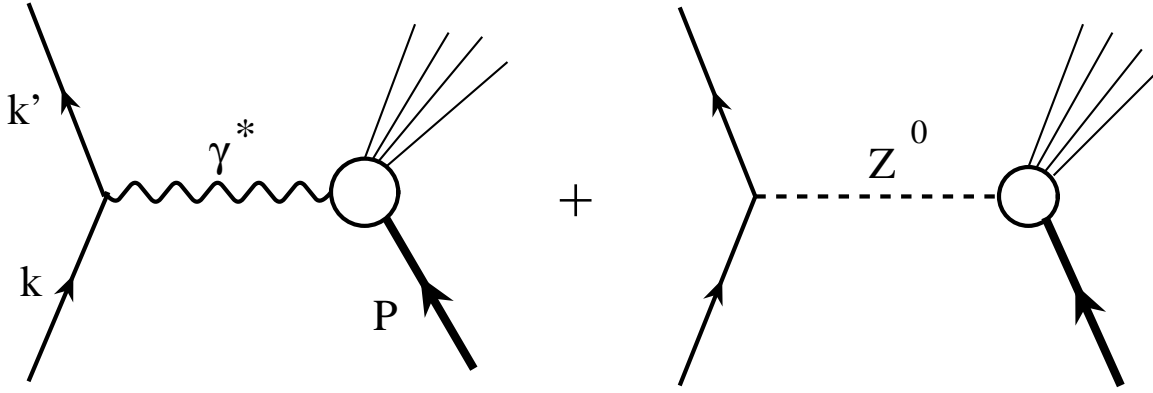


Figure 1: First order Feynman diagrams for lepton-nucleon scattering in the presence of a weak neutral current.

scattering, the weak cross section is much smaller than the electromagnetic cross section, so the former can be safely neglected. However, the electromagnetic part is parity conserving, so the cross section is the same for right and left handed electrons, while the neutral current amplitude contains a parity violating term. Consequently the weak neutral current can be measured using the parity-violating asymmetry in the inclusive cross sections for electrons polarized parallel (R) and anti-parallel (L) to their momentum. The PV asymmetry is given by

$$A_{RL} = \frac{d\sigma_R - d\sigma_L}{d\sigma_R + d\sigma_L}. \quad (2)$$

Here  $d\sigma_R$  and  $d\sigma_L$  are the cross sections for scattering right and left handed electrons off an unpolarized target.

## 2.2 Resonance Region Asymmetry

In the nucleon resonance region, it is possible to describe  $A_{RL}$  in terms of response functions to specific final states, combined with a non-resonant background. In the one gauge boson ( $\gamma$  or  $Z^0$ ) exchange approximation the asymmetry for scattering to discrete states can be written as [17, 18],

$$A_{RL}^{Res} = A_0 \frac{v_L R_{AV}^L(q, \omega) + v_T R_{AV}^T(q, \omega) + v_{T'} R_{VA}^{T'}(q, \omega)}{v_L R^L(q, \omega) + v_T R^T(q, \omega)}, \quad (3)$$

where  $L$ ,  $T$ , and  $T'$  stand for longitudinal, transverse, and axial, and  $v_{L,T}$ 's are lepton kinematic factors. The term  $A_0 \approx 6.5 \times 10^{-4}$  [17] and the subscripts  $AV$  and  $VA$  denote axial-vector leptonic and vector hadronic currents and vector leptonic and axial-vector hadronic currents. The parity violating responses  $R_{AV}^{L,T}$  can be decomposed in terms of their isospin content [17],

$$R_{AV}^{L,T} = \beta^{I=0} R_{L,T}(I=0) + \beta^{I=1} R_{L,T}^N(I=1), \quad (4)$$

$$\beta^{I=0} = -2 \sin^2 \theta_W, \quad \beta^{I=1} = (1 - 2 \sin^2 \theta_W), \quad (5)$$

and  $I$  is the isospin quantum number. In the case of  $N(1520)$ , which is an isospin  $\frac{1}{2}$  state, both terms in equation (5) contribute to the asymmetry. If one makes the approximation  $\sin^2(\theta_w) = 0.25$  (so that the vector leptonic current, which multiplies the axial hadronic current, is zero), then in the limit of pure magnetic or electric scattering, and assuming isospin symmetry and negligible strange and charm form factors, the proton asymmetry can be written as:

$$A_{RL}^{Res,p} = -0.9 \times 10^{-4} Q^2 \frac{\sigma_n}{\sigma_p}, \quad (6)$$

a remarkably simple equation. For the deuteron, the result has a different sensitivity to nuclear structure and with these approximations becomes:

$$A_{RL}^{Res,d} = -0.9 \times 10^{-4} Q^2 R(W). \quad (7)$$

where  $R(W)$  depends on the relative  $I = 1$  compared to  $I = 0$  strength, and is unity for a pure  $I = 1$  transition, and is negative for a pure  $I = 0$  transition.

We stress that these simplified relations are simply presented here to bring out the main features of the PV asymmetry, and that the terms we are neglecting (axial current, strange and up/down sea quarks) are interesting and will be fully addressed in the actual data analysis.

Although the formalism for this was worked out long ago [19], to the best of our knowledge the details have so far only been worked out for the case of elastic scattering [20] and the  $N \rightarrow \Delta(1232)$  transition [21], although there is an ongoing effort to understand the higher  $W$  region [17], in particular the influence of meson exchange currents. An approximate model for the  $S_{11}(1530)$  resonance was very recently presented in the Ph.D. thesis of Sacco [22].

A detailed prediction of the  $N \rightarrow \Delta(1232)$  proton asymmetry is given by [21]  $A_p^\Delta = -(1.04 + 0.27F(Q^2, E, E', \theta_e) \times 10^{-4} Q^2$  where  $F(Q^2, E, E', \theta_e)$  contains the information on weak form transition form factors, and is expected to be of order unity for  $Q^2 < 1$  GeV<sup>2</sup>, decreasing to zero at very large  $E$  (or small  $Q^2/2ME$ ) [20]. In the moderate  $Q^2$  and energy of this proposal, this detailed prediction is within 20% of the simple model given by Eq. (6), since  $\sigma_n/\sigma_p = 1$  for the isovector  $\Delta(1232)$  resonance.

### 2.3 Deep-Inelastic Asymmetry

In the Standard Model and assuming quark degrees of freedom, the asymmetry arises from the interference between photon and  $Z$  exchange diagrams, and is given by [20]

$$A = \frac{\sigma_R - \sigma_L}{\sigma_R + \sigma_L} = -\frac{2Q^2}{M_Z^2} \frac{\sum f_i(x)(Q_i^\gamma/e)[g_A^e g_V^i + Y g_V^e g_A^i]}{\sum f_i(x)(Q_i^\gamma)^2}, \quad (8)$$

where  $f_i(x)$  are the quark distribution functions for a quark of type  $i$ , the  $g$ 's are the electroweak axial and vector charges,  $Q^2 = -q^2$  is the four-momentum transfer squared

( $Q^2 > 0$  for our kinematics),  $M_Z$  is the mass of the  $Z$  boson, and

$$Y = \frac{1 - (1 - y)^2}{1 + (1 - y)^2 - y^2 R / (1 + R)} \quad (9)$$

where  $y = \nu/E$ ,  $\nu = E - E'$  is the energy lost by an incident electron of energy  $E$  scattering to an electron of energy  $E'$ , and the factor  $R = \sigma_L/\sigma_T$  takes into account [23] the longitudinal contributions to both  $Z$  and photon exchange. Performing the sums and re-writing  $M_Z$  in terms of the  $\alpha$  and  $G_F$  coupling constants, for a proton target we obtain

$$A_p = \frac{3G_F Q^2}{\pi\alpha 2\sqrt{2}} \frac{2C_{1u}[u(x) + c(x)] - C_{1d}[d(x) + s(x)] + Y[2C_{2u}u_v(x) - C_{2d}d_v(x)]}{4u(x) + d(x) + s(x) + 4c(x)}. \quad (10)$$

where the products of weak charges in the Standard Model at tree level are given by:

$$\begin{aligned} C_{1u} &= g_A^e g_V^u \\ C_{1d} &= g_A^e g_V^d \\ C_{2u} &= g_V^e g_A^u \\ C_{2d} &= g_V^e g_A^d. \end{aligned} \quad (11)$$

When Standard Model electroweak radiative corrections are included the  $C_{ij}$  become [24]

$$\begin{aligned} C_{1u} &= \rho' \left( -\frac{1}{2} + \frac{4}{3} \kappa' \sin^2(\theta_w) \right) + \lambda_{1u} \approx -0.1886 \\ C_{1d} &= \rho' \left( \frac{1}{2} - \frac{2}{3} \kappa' \sin^2(\theta_w) \right) + \lambda_{1d} \approx 0.3414 \\ C_{2u} &= \rho \left( -\frac{1}{2} + 2\kappa \sin^2(\theta_w) \right) + \lambda_{2u} \approx -0.0359 \\ C_{2d} &= \rho \left( \frac{1}{2} - 2\kappa \sin^2(\theta_w) \right) + \lambda_{2d} \approx 0.0265. \end{aligned} \quad (12)$$

In the limit of no electroweak radiative correction  $\rho = \rho' = \kappa = \kappa' = 1$  and  $\lambda_{1u} = \lambda_{1d} = \lambda_{2u} = \lambda_{2d} = 0$ .

We have assumed that the  $u(x)$ ,  $d(x)$ ,  $s(x)$ , and  $c(x)$  quark parton distribution functions (PDFs) of the proton can be described in terms of valence ( $v$ ) and sea ( $s$ ) contributions as

$$\begin{aligned} u(x) &= u_v(x) + u_s(x) + \bar{u}_s(x) \\ d(x) &= d_v(x) + d_s(x) + \bar{d}_s(x) \\ s(x) &= s_s(x) + \bar{s}_s(x) \\ c(x) &= c_s(x) + \bar{c}_s(x) \end{aligned} \quad (13)$$

The quark distribution functions depend mainly on the Bjorken scaling variable  $x = Q^2/2M\nu$  (where  $M$  is the nucleon mass), but also evolve slowly with  $Q^2$  due to QCD

and finite mass corrections. While not shown explicitly, all quantities involving PDFs are functions of both  $x$  and  $Q^2$ .

In the valence region,  $A_p$  is numerically approximated using Eq. (10) and Eq. (12) by

$$A_p = -10^{-4} Q^2 \frac{[0.51 + 0.45r(x) + 0.10Y(1 + r(x))]}{[1 + 0.25r(x)]}, \quad (14)$$

where we have ignored the strange and charm quark contributions,  $r(x) = d(x)/u(x) \approx 1 - 0.75x$ , and  $Q^2$  is in units of  $\text{GeV}^2$ . Using isospin symmetry and with the approximation  $\sin^2(\theta_w) = 0.25$ , and ignoring strange and charm quark contributions, this can be written as

$$A_p = -0.9 \times 10^{-4} Q^2 \frac{2(1 + \sigma_n/\sigma_p)}{5}. \quad (15)$$

The full equation for the deuteron asymmetry is given by

$$A_d = -10^{-4} Q^2 \frac{[0.78 + 0.41R_c(x) + 0.37R_s(x) + 0.10YR_v(x)]}{[1 + 0.2R_s(x) + 0.8R_c(x)]}, \quad (16)$$

which when simplified in the valence region using  $\sin^2(\theta_w) = 0.25$ , can be written as

$$A_d = -0.7 \times 10^{-4} Q^2, \quad (17)$$

which is about 20% less than the simplified transition form factor model for a pure  $I = 1$  transition.

## 2.4 Duality

Quark-hadron duality was first observed by Bloom and Gilman in 1970 [6]. It postulates that physical quantities calculated in the hadronic description give the same results as if they were calculated using the partonic description if a proper scaling variable that connects the two kinematic regions is used. In QCD, De Rujula, Georgi and Politzer [5] have shown that duality can be understood from an operator product expansion of moments of structure functions, which allows one to separate the short and long distance contributions to the moments of structure functions. The leading terms in the OPE correspond to scattering from free quarks, which are responsible for scaling, while higher terms take interactions between quarks and gluons (higher-twists) into account. In the resonance region if the higher-twists are significant then the moments of structure functions cannot be much different than the corresponding scaling value, which is given by the moments of the leading-twist term. Therefore, if a structure function rises above the scaling value it has to fall in the neighboring region (or oscillate around the scaling function) in order to compensate for the increase or decrease in the moments above the scaling value. This explains why resonances average to a smooth scaling curve. This behavior observed over restricted regions in  $W$  for each resonance is known as local duality. So far duality has been seen to work for unpolarized structure functions for the electromagnetic tensor,  $W_1^{EM}$  and  $W_2^{EM}$ , to  $Q^2$  as low as  $0.6 \text{ GeV}^2$ . Figure 2

shows the structure function  $\nu W_2^{EM}$  as a function of the Nachtmann scaling variable,  $\xi = 2x/[1 + \sqrt{1 + 4x^2 M_N^2/Q^2}]$ , for different  $Q^2$  values. The data clearly demonstrate that duality works remarkably well to rather low values of  $Q^2$ .

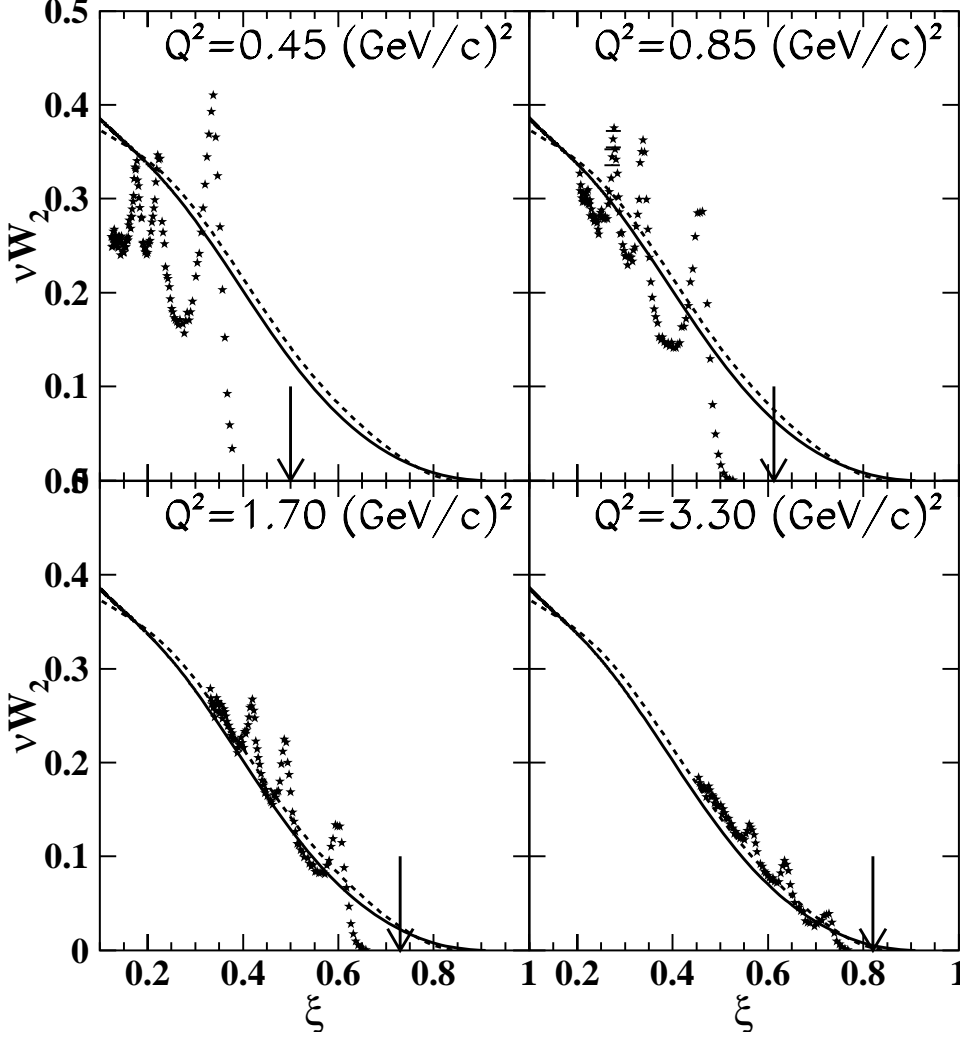


Figure 2: The spin independent structure function  $\nu W_2^{EM}$  plotted as a function of  $\xi$  for hydrogen at different  $Q^2$  values [7]. The solid and dashed lines are a fit to deep inelastic structure function data at  $Q^2 = 10$  ( $\text{GeV}/c^2$ ) and  $Q^2 = 5$  ( $\text{GeV}/c^2$ ) respectively.

In terms of structure functions, to lowest order in the weak and electromagnetic currents,  $A_{RL}$  can be written as,

$$A_{RL} = \frac{Q^2}{Q^2 + M_Z^2} \frac{g_A(2W_1Q^2 + W_2(4EE' - Q^2)) - g_v W_3 Q^2 (E + E')/M}{2W_1^{EM}Q^2 + W_2^{EM}(4EE' - Q^2)}, \quad (18)$$

where  $W_{1,2,3}$  are structure functions for the interference tensor of the electromagnetic and weak neutral hadron currents,  $g_v$  and  $g_A$  are the vector and axial-vector coupling

constants at the lepton- $Z^0$  vertex and  $E$  and  $E'$  are the energies of the incoming and outgoing electron. The denominator of the asymmetry  $A_{RL}$  depends only on  $W_1^{EM}$  and  $W_2^{EM}$ . Both these structure functions are very well measured and understood at the  $Q^2$  values of this experiment and can be determined using a model. Although it is not possible to separate the structure functions for the interference tensor,  $A_{RL}$  can be used to test duality for a linear combination of  $W_1$ ,  $W_2$  and  $W_3$  (numerator of Eq. (18)). Duality has never been tested for these structure functions to the date. As pointed out in the previous section depending on the isospin of the final excited state the interference cross section is expected to show a resonance structure.

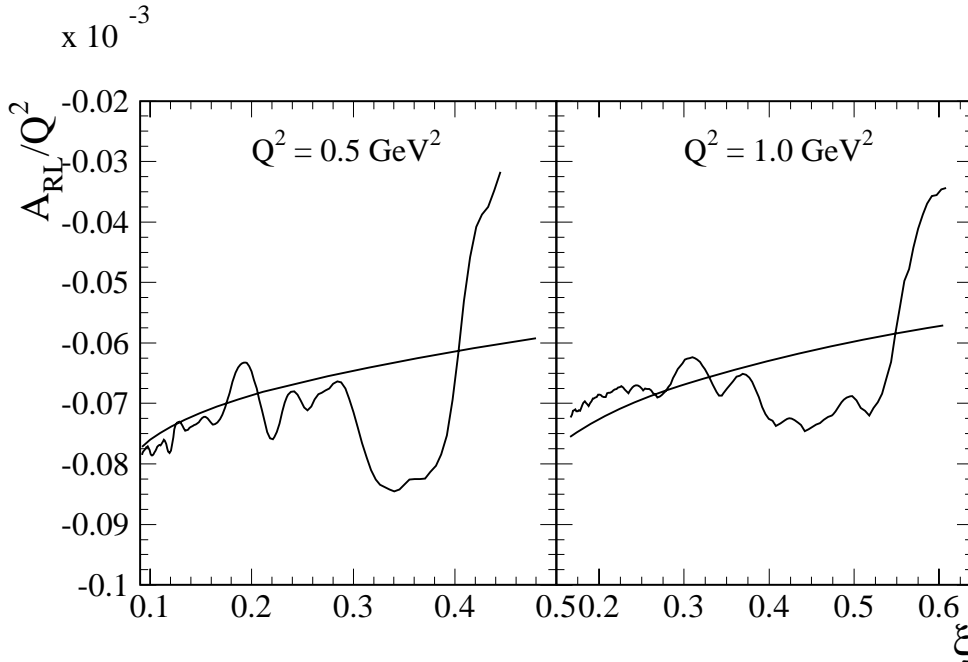


Figure 3: The oscillating curves are the simplified resonance region prediction for  $A_p(W, Q^2)$  in the limit  $\sin^2(\theta_w) = 1/4$  from Eq. (6) using a fit [25] for  $\sigma_n/\sigma_p$ . The smooth curves are the DIS prediction from Eq. (14).

Figure 3 shows the expected asymmetry for the proton calculated with the simplified model of Eq. (6) and a fit [25] to  $\sigma_n/\sigma_p$ , at the two average  $Q^2$  values of this proposal. Also shown is the DIS prediction, evaluated at the corresponding values of  $\xi$ , and a standard set of PDFs for  $d(x)/u(x)$  to evaluate  $\sigma_n/\sigma_p$ . It can be seen that in this approximate model, duality appears to roughly work at both the local and global level. Essentially, the leading order criteria for duality to work can be written as

$$(\sigma_n/\sigma_p)^{res} = \frac{2}{5} \left( 1 + (\sigma_n/\sigma_p)^{DIS} \right) \quad (19)$$

The two different dependencies on  $\sigma_n/\sigma_p$  come from the fact that in the resonant case, the current is expressed through the square of the sum over parton charges, while in the

DIS limit, it is the sum of the squares which gives the current. As pointed out by Close and Isgur [26], the cross terms can cancel on average when opposite parity states are mixed. In Fig. 3 it can be seen that the average of the  $\Delta(1232)$  and the elastic peak region tend to equal the DIS curve, and that at higher masses there are many resonances whose sum appears to oscillate around the DIS limit. We note that Eq. (19) is satisfied if on average  $\sigma_n/\sigma_p = 2/3$ , which is not a bad approximate of actuality.

In the case of the deuteron, the simplified formulas Eq. (7) and Eq. (17) differ by 20% for  $R(W) = 1$  (as for the  $N \rightarrow \Delta$  transition in the absence on non-resonant background terms). On the other hand, the average of the quasi-elastic and  $\Delta(1232)$  asymmetries lies close to the DIS prediction.

Only with experimental data (which will include the effects of the axial current, strange form factors and higher twist contributions) will we be able to tell if duality works in actuality, and to what accuracy it works. Duality in the unpolarized  $F_2$  structure function is good to  $\sim 5\%$  down to  $Q^2=0.5$  GeV<sup>2</sup>, and we will be able to make tests of local duality with comparable precision, and global duality down to 2-3%. A quantitative understanding of duality in PV electron scattering will provide new constraints for models trying to understand duality and its QCD origins. In addition, if duality is observed to hold at the few percent level at the lower  $W^2$  and  $Q^2$  values of this measurement, it would provide significant limits on the contributions of higher twists to DIS-parity measurements at 6 and 11 GeV.

### 3 Experiment

The primary goal of the experiment is to measure  $A_p$ ,  $A_d$ , and  $A_C$  in and slightly beyond the traditional nucleon resonance region ( $M < W < 2.1$  GeV) at moderate  $Q^2$ . The choice of hydrogen and deuterium as the targets is dictated by the desire to observe possible resonance structure, without the large blurring effects of Fermi motion and shadowing in heavier nuclei, and to test duality using the weak neutral current with two isospin combinations, for which the predictions are quite different, as was discussed above. Measurements with both hydrogen and deuterium have a further advantage, in that the ratio of asymmetries is almost free of experimental systematic errors, allowing a very precise comparison with theory. The data on carbon allows a first look at the nuclear dependence in PV electron scattering, while also providing input for cross sections models needed in precise neutrino scattering measurements and backgrounds for other PV electron scattering measurements.

The range of  $Q^2$  to be explored is limited to about 0.5 GeV<sup>2</sup> on the low end due to increasingly large elastic radiative tails at low  $Q^2$  (which dilute the measured asymmetry), and by the smallest practical scattering angle for a large solid angle spectrometer. The range of  $Q^2$  on the high end is limited to about 1 GeV<sup>2</sup> by the beam energy and the rapidly decreasing cross sections with increasing  $Q^2$ . The range of  $0.5 < Q^2 < 1$  is well matched to that where the onset of duality is seen to occur in the spin-averaged proton response functions, as well as the spin-dependent structure function  $g_1$  [9]. We have picked an average  $Q^2$  of 0.8 GeV<sup>2</sup> as giving the best sensitivity to the physics issues

we wish to study.

The experimental asymmetry is diluted by the beam polarization  $P_e$ , so that

$$A_{exp} = \frac{N_+ - N_-}{N_+ + N_-} = P_e A,$$

where  $N_+$  and  $N_-$  are the number of scattered electrons detected from + and - beam helicities respectively. The statistical uncertainty is given by

$$\delta A = \frac{1}{P_e \sqrt{N_+ + N_-}}.$$

For  $Q^2$  in the 1 GeV<sup>2</sup> range, on the order of 10<sup>12</sup> electrons must be detected to achieve a 1% uncertainty in the physics asymmetry.

For  $Q^2 = 1$  GeV<sup>2</sup>, typical asymmetries are of order 100 ppm, large compared to the typically few ppm asymmetries of HAPPEX or G0 experiments at JLab, and comparable to the raw asymmetries measured in Hall B with polarized electrons incident on polarized deuterons in ND3. This makes the requirements on beam systematics for this proposal (charge and position asymmetries and jitter, leakage from other Halls, etc.) considerably more relaxed than in previous PV experiments at JLab.

### 3.1 Optimization of Kinematics

Several considerations enter into the optimization of beam energy and spectrometer angle. The beam energy  $E$  must be at least 3 GeV to span the full resonance region. In practice, a higher beam energy of 4 GeV is needed to avoid large radiative tails at high  $W$ . For a given choice of  $Q^2$ , the figure of merit (FOM) improves approximately linearly with  $E$ , due to the larger cross section at the correspondingly smaller angles. However, the maximum momenta of the HRS spectrometers (3.2 and 4.3 GeV) limits the useful beam energy to 5.1 GeV. If we lower this to 4.8, we can take two settings with each spectrometer and have overlap between the higher and lower  $W$  settings. The best figure of merit is then obtained by running at the smallest possible angle that doesn't require the septum magnets, which is 12.5 degrees.

### 3.2 Beam Line and Polarimetry

We propose to use 4.8 GeV polarized beam with a 80% polarization and 85  $\mu$ A beam current. To reduce the heat impact on the target, the beam is circularly rastered such that the beam spot size at the target is  $\approx 4$  mm in diameter (or rectangularly rastered to a 4 $\times$ 4 mm<sup>2</sup> spot). The beam energy can be measured to a  $\Delta E/E = 2 \times 10^{-4}$  level using either ARC or eP devices [27]. The beam polarization will be measured by the Compton polarimeter utilizing a upgraded (green) laser. Compton-scattered electrons and photons are detected by two sets of detectors and the data can be analyzed either inclusively or in coincidence. The systematic error of "electron only" method for a 4.8 GeV beam is 1.1%. Within 40 minutes of 85  $\mu$ A beam the statistical error is 0.6%, giving a total error of

1.2%. The systematic error of “photon integration” method currently being developed by the HAPPEX collaboration is also expected to achieve a 1% level, providing a cross check of the electron method. The green laser upgrade of the Compton is already underway. It is expected to be installed in the hall in 2006 and will be used for two approved experiments PREX [28] and DIS-parity [29].

### 3.3 Parity DAQ (Hall A)

The parity DAQ in Hall A [30] and the beam helicity feedback system have been successfully used to control the beam helicity-dependent asymmetry for the Hall A parity experiments in the past. The asymmetry in the integrated beam current measured by the parity DAQ is sent to the polarized electron source where the Pockel cell voltage is adjusted accordingly to minimize the beam intensity asymmetry. Using this method the beam helicity asymmetry was controlled to the  $10^{-7}$  level during HAPPEX. Since the false asymmetry caused by the beam helicity asymmetry is a second order effect hence is much smaller than the latter, and our measured asymmetry is much bigger than that measured by HAPPEX, we request that the beam helicity asymmetry to be controlled below  $10^{-6}$  which will require only modest effort.

### 3.4 The Liquid Target

We choose to use two racetrack-shaped 25 cm long cells with 5 mil aluminum for both entrance and exit windows. One cell will be filled by LD2 and the other by LH2. A  $2.5 \text{ g/cm}^2$  carbon target (6% radiation length) will be added to the target ladder.

The target will be almost identical to the one used by HAPPEX in 2004-5, aside from the additional cell. Cooling from the CHL is piped in to aid the ESR. The racetrack-shape is chosen because of its much smaller boiling effect than the commonly used cigar-shape (cylindrical) cells. Boiling tests on racetrack-shaped LH2 cells were performed by the HAPPEX collaboration in 2004 [31], where a negligible boiling noise ( $< 100$  ppm) was found for a 20-cm long LH2 cell and a  $70 \mu\text{A}$  beam. A  $5 \times 5 \text{ mm}^2$  raster and 60 Hz fan speed were used for the test. The boiling noise of a LD2 cell is expected to be at the same level, and will not be a problem for the proposed measurement. Boiling tests on a LD2 cell will be performed during commissioning to optimize the running condition. We plan to start from a  $4 \times 4 \text{ mm}^2$  raster and 60 Hz fan speed and the boiling noise will be measured up to a beam current of  $90 \mu\text{A}$ . Such a test is also a pre-requisite for the approved DIS-parity experiment.

### 3.5 Luminosity Monitor

The luminosity monitor (Lumi) in Hall A was successfully used for the HAPPEX experiment in their 2004 and 2005 run, and will be used for the two approved experiments PREX and DIS-parity. In the following we discuss how well the noise level can be controlled by the Lumi.

The Lumi consists of 8 pieces of quartz at  $0.5^\circ$ . Each piece has  $2 \times 5 \text{ cm}^2$  effective area at 7 m from target. The rate for 4.8 GeV beam is  $> 10^{11}$  Hz per piece. With this high rate, the false asymmetry and the target boiling effect has been monitored to a level of 100 ppm per pulse during the 2004 running of HAPPEX II for a  $70 \mu\text{A}$  current and a  $5 \times 5 \text{ mm}$  raster. With a  $85 \mu\text{A}$  current and a  $4 \times 4 \text{ mm}$  raster being proposed here, the noise level is expected to be controlled below the  $10^3$  ppm level, thus will add negligible effect to the statistical width of the measured asymmetry (0.01 per pulse).

Most of the events in Lumi are elastic. The asymmetry is in general proportional to  $Q^2$ , hence the physics asymmetry detected by Lumi is very small, of the order of  $< 100$  ppb. Therefore the false asymmetry can be monitored to  $\approx 100$  ppb. Compared to the physics asymmetry that we proposed to measure ( $50 \sim 100$  ppm), this will cause a  $< 0.2\%$  systematic uncertainty and is therefore negligible.

### 3.6 Spectrometers and Pole-tip Background

We use the standard Hall A High Resolution Spectrometer (HRS) to detect the scattered electrons. For each HRS the effective solid angle acceptance for an extended target is 6 msr and the momentum bite is  $\pm 4.5\%$ . The central momentum of the HRS can be calculated from the dipole field magnitude at the  $5 \times 10^{-4}$  level [27]. The HRS central angle can be determined to  $\pm 0.2$  mrad with careful analysis [32].

One of the concerns of most parity experiments utilizing spectrometers is the Møller-scattered electrons off the magnetized iron inside the spectrometer magnet (“pole-tip” background). This has been studied extensively by the HAPPEX collaboration. During their test runs, the angle of one spectrometer was set slightly away from the elastic peak such that elastically scattered electrons may hit the pole-tips. Such events are then tagged by the elastically scattered protons in the other spectrometer. Using this method an upper limit on the asymmetry from pole-tip events was found to be  $\delta A < 10^{-8}$  [33]. Simulations were also performed to confirm this test result and in fact, the background asymmetry was found to be less than  $2 \times 10^{-9}$  in the simulation [34]. We scale the HAPPEX number by the ratio of electron flux, detector acceptance, also consider that not all pole-tip events can survive the event selection of the DAQ, and find the pole-tip background for the proposed measurement to be  $\delta A < 7 \times 10^{-8}$ . Compared to the  $50 \sim 100$  ppm measured asymmetry, this contribution is  $< 0.2\%$ .

### 3.7 Particle Identification Detectors

Particle identification (PID) in each HRS will be done with a  $\text{CO}_2$  Cerenkov detector and a double-layered lead glass shower detector. Based on data from past experiments, the combined pion rejection factor of these two detectors was found to be  $\geq 10^4$  [35] for a given electron efficiency of  $\geq 99\%$  each. At high rate, a practical estimate of the PID efficiency should also take into account the effect of event pileup, detector readout deadtime and electronic noise. We simulated these effects and the pion rejection with the fast counting DAQ is found to be better than  $10^3$ .

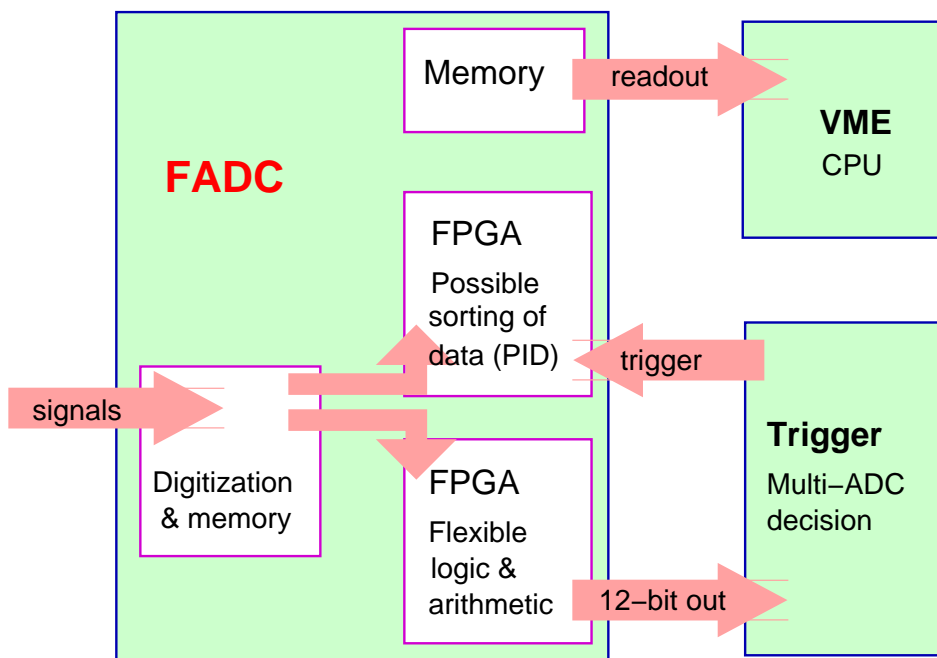
### 3.8 Fast Counting DAQ

To separate the pion background we will use a counting method. The counting method has been used successfully at 100 MHz by the Mainz A4 parity violation experiment [36, 37]. Also relevant is the experience of the G0 collaboration in deploying a counting method [38]. We plan to use a Flash ADC (FADC)-based fast counting DAQ which has virtually no deadtime, and use a scaler-based DAQ as cross check. This strategy will also be used for the DIS-parity experiment and test runs of both DAQs using a small fraction of the PID detectors are already underway by the DIS-parity collaboration. The basic principle of these two DAQs is described below:

#### 3.8.1 FADC-based DAQ

Figure 4: Schematic diagram for the fast DAQ system (a possible 2<sup>nd</sup> generation of JLab in-house design).

250 MHz, 2 usec latency, 1 MHz on-board analysis, 0.1% DT measurement



The detector signals we will use include the 10 PMT signals from the gas Cherenkov detector and the approximately 180 signals from two layers of lead glass detectors. To reduce the processing time and the noise, as well as the number of FADC modules, both detectors will be segmented. PMT signals from each segments are summed first and then sent to the FADC for digitizing. Segmentation of the detectors will also allow binning

in the  $W$  and  $Q^2$ , the central value of which can be checked by taking data with regular HRS DAQ at low rates. In addition, the 24 signals from scintillators might be useful for crude directional information.

For the FADC we are considering a modified version of the one presently being designed by the Fast Electronics Group at JLab. A schematic diagram is given in Fig. 4. This FADC design will allow for the possibility of counting experiments at approximately 1 MHz with virtually now deadtime. The FADC fills an on-board memory at 250 MHz with  $\approx 4 \mu\text{sec}$  latency (buffer size). The information provides both amplitude and timing information about the signal. An on-board processor (FPGA) will analyze the digitized data, with intermediate results sent to an external trigger processor to form a trigger based on multiple FADC boards. The scheme will be flexible enough to accommodate a variety of experiments. A first version of the FADC should be ready by 2007.

The on-board algorithm shall permit an online identification of electrons, pions, and associated pileup, and counts these in local memory on the FADC. The data which is read out from the FADCs by the VME cpu is the number of counts of these particles integrated over the helicity pulse, usually at 30 Hz, and possibly at a higher sampling rate, say 600 Hz. In a test mode the entire FADC data may be read (at the price of some deadtime) to check the reliability of the algorithm.

Electrons are identified as events which pass above the Cherenkov cut and which deposit a sufficient total energy in the lead glass, while pions leave no signal in the Cherenkov and small average signals in the lead glass. The efficiency of the cuts and the cross contamination of the particle samples can be checked at very low beam current. From experience in Hall A, these efficiencies and contaminations are already known under running conditions similar to the proposal. Pileup of two particles will occur in approximately 6% of events if we make no changes to the existing phototubes which have a 60 nsec resolving time. Although these effects are not easy to study directly at high rates, we can indirectly study them by an analysis in which the data of independent events are added. The pileup effects include: 1)  $e^- - e^-$ ; 2)  $e^- - \pi$ ; 3)  $\pi - \pi$ . Since electrons must only pass a threshold, electrons accompanied by a secondary particle will still be counted as electrons; however, a correction must be applied for two-electron pileup. These can be measured using a higher threshold cut on the lead glass and counting the events that pass this higher threshold. For the lowest momentum setting of the proposed measurement where the  $\pi/e$  ratio is the highest, a total rate of 1.3 MHz (800kHz  $e^-$  and 500kHz  $\pi^-$ ), the pileup involving pions will result in a (1.5 – 2.0)% loss of the pion count rate, since they tend to be moved away from the one-pion cut window. A fraction (0.5 – 1)% of two pion events will be counted erroneously as electrons. These effects from pions can be corrected with sufficient accuracy and the uncertainty is practically negligible (since the  $\pi/e$  ratio and the pion asymmetry will be measured precisely).

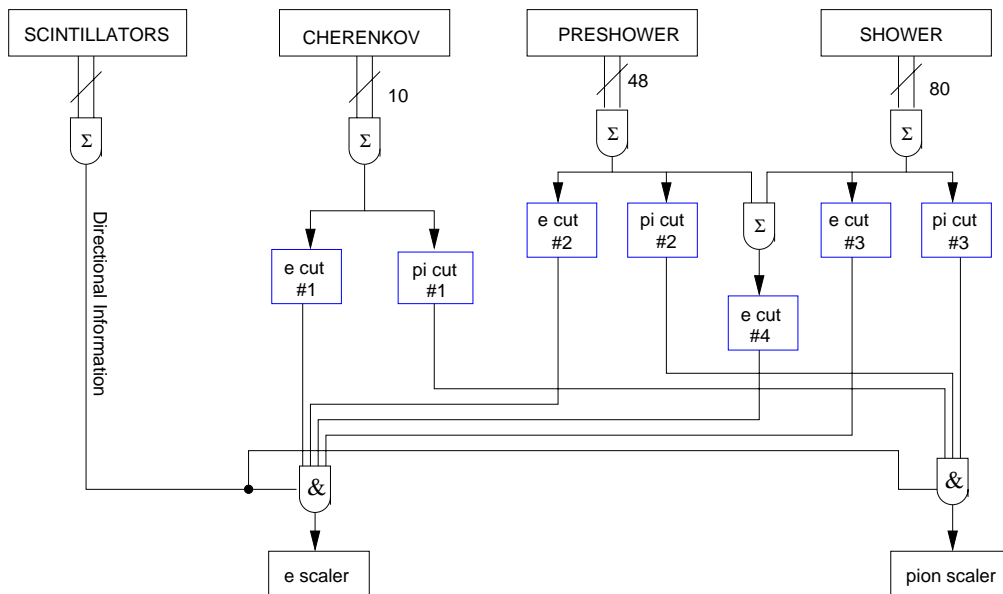
If the processing of the FADC is fast enough we can maintain a deadtime which is very small, probably  $\leq 10$  nsec. However, the system may have a deadtime of order 1% which could be different for different physical processes. Our goal is to measure the deadtime correction to the physics asymmetry with an absolute accuracy  $\pm 0.3\%$ . To ensure reliability it is important to measure the deadtime with at least two independent

methods as follows. A first method is to pulse the detector channels with a light sources whose amplitude and pulse shape is similar to those of real particles, and count how many of these signals are subsequently identified by the electronics. A second method is to introduce a deliberate programmed deadtime into the frontend, thus making it predictable and understood.

### 3.8.2 Scaler-based DAQ

An alternative way to count events is to use a custom scaler electronics. The electronics will process signals from PID detectors and scintillators and perform a fast on-line discrimination. Useful electrons, pions, and two-electron pileup events will be identified using different discrimination thresholds, see Fig. 5.

Figure 5: PID Logic diagram for the scaler-based DAQ.



To ensure the stability of this scaler electronics, the outputs of a typical module need to be wide enough, typically 20 ns, causing a deadtime of 2.4% for 1.2 MHz rate. We plan to measure this deadtime also to an absolute accuracy of  $\pm 0.3\%$  using the same methods as described above for the FADC DAQ. More importantly, it will provide a reliable online check of the FADC counting both for data taking at high rates and test runs at low rates. If any inconsistency is observed between the two DAQs, one can investigate possible problems promptly. For example, full-sampling FADC data can be collected to diagnose whether there is a problem with the FPGA algorithm.

Table 1: Kinematic variables, pion/electron ratio, total particle rate (electron plus pion), expected asymmetry (DIS model), and expected relative asymmetry error for the proposed measurements. All data is taken with a beam energy of 4.8 GeV and a scattering angle of  $12.5^\circ$ .

$W$ (GeV)	$x$	$Q^2$ (GeV <sup>2</sup> )	$Y$	$E'$ (GeV)	$\pi/e$	rate (MHz)	$A$ (ppm)	$dA/A$ (%)
LH2								
2.00	0.17	0.64	0.50	3.0	0.5	0.5	46	9.1
1.78	0.24	0.73	0.39	3.2	0.2	0.5	51	7.4
1.52	0.36	0.82	0.29	3.6	0.1	0.6	53	5.7
1.21	0.61	0.91	0.19	4.0	0.0	0.8	52	4.9
LD2								
2.00	0.17	0.64	0.50	3.0	0.6	0.8	61	6.2
1.78	0.24	0.73	0.39	3.2	0.2	0.9	64	5.1
1.52	0.36	0.82	0.29	3.6	0.1	0.9	67	4.5
1.21	0.61	0.91	0.19	4.0	0.0	1.3	71	3.4
Carbon								
2.00	0.17	0.64	0.50	3.0	0.6	0.5	61	8.1
1.78	0.24	0.73	0.39	3.2	0.2	0.5	64	6.6
1.52	0.36	0.82	0.29	3.6	0.1	0.5	67	5.9
1.21	0.61	0.91	0.19	4.0	0.0	0.9	71	4.4

## 4 Expected Results

### 4.1 Kinematic Coverage

The kinematic coverage in  $W$ ,  $Q^2$ ,  $x$ , and  $Y$  is shown in Table 1. The full resonance region  $M < W < 2.1$  GeV is covered, with an average  $Q^2$  of 0.8 GeV<sup>2</sup> for  $E = 4.8$  GeV. Figure 6 shows the distribution of events at the HRS calorimeter for the  $P_{HRS} = 3.2$  GeV setting. Each calorimeter block covers 14.5 cm, corresponding to a  $W$  bin of less than 25 MeV per block (full width). The  $W$  resolution is slightly worse at larger  $E'$  values, with a worst case value of 50 MeV (full width) near the peak of the  $\Delta(1232)$  resonance.

### 4.2 Statistical and Systematic Uncertainties

The expected statistical errors are listed in Table 1. We will divide each spectrometer setting into two (or more)  $W$  bins. Resonant structure on the scale of 10% will be clearly visible with these data: this is small compared to the 30% to 50% resonant fluctuations

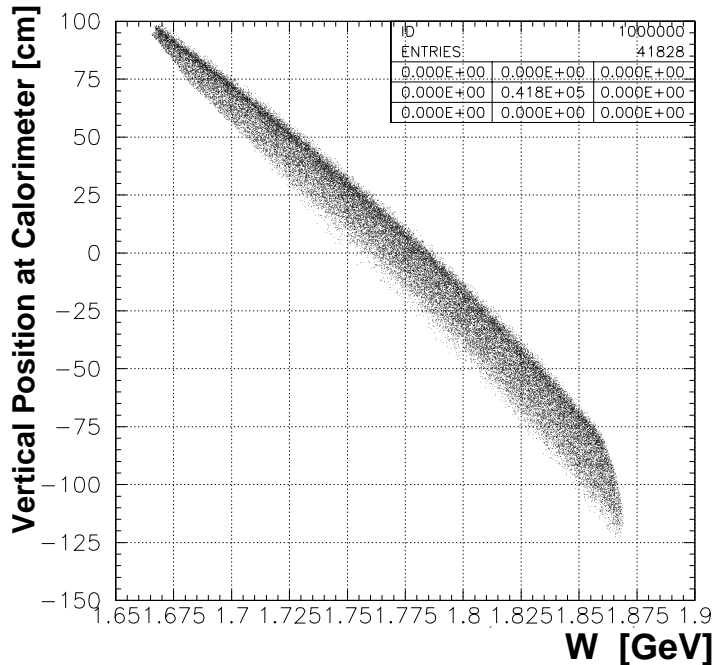


Figure 6: Missing mass  $W$  as a function of vertical position at the calorimeter for the  $E' = 3.2$  GeV setting.

of the unpolarized structure functions around the smooth duality curve. For tests of local duality, we can divide the full resonance region into four regions in  $W$ , and in each region will be able to test local duality at the level of about 4%. This seems quite adequate for a pioneering measurement. At these  $Q^2$  values, duality in the unpolarized structure function is good to  $\sim 5\%$ , so this measurement will be able to determine if duality in parity violating electron scattering is of a similar quality or if there are significantly larger deviations. This information, coupled with recent measurements of duality in longitudinal, transverse, and spin-dependent structure functions will provide additional input to efforts aimed at understanding the origin of duality in QCD.

The statistical error for a test of global duality (averaged over the entire resonance region) will be at the level of 2%, which is well-matched to the anticipated systematic error (see below). The error on the ratio of averaged proton, deuteron, and carbon asymmetries will be about 3%, with a much smaller systematic error, since the largest sources of systematic uncertainty cancel in the ratio.

The expected systematic errors are tabulated in Table 2, and discussed in the following sub-sections.

Table 2: Estimated experimental systematic errors on  $dA/A$ . Note that in the comparison of proton, deuteron, and carbon, the uncertainties in the beam polarization and  $Q^2$  determination will largely or completely cancel, yielding a systematic of  $\approx 0.010$  for the target ratios.

source	$\delta A/A$
Beam Polarization	0.012
Kinematic determination of $Q^2$	$<0.009$
Deadtime corrections	0.003
Electromagnetic radiative corrections	0.005
Beam asymmetries	0.005
Pion contamination	$<0.005$
Pair symmetric background	0.002
Target purity, density fluctuations	0.002
Total	$<0.018$

### 4.3 Beam Polarization

We will use the Hall A Compton polarimeter, as described in section 3.2. With the upgraded polarimeter being developed for PREX [28] and DIS-parity [29], we will achieve a 1.2% measurement of the beam polarization. The PREX experiment is planning an upgrade of the Møller polarimeter to achieve a 1% measurement. We will use this as a cross check for the Compton polarimeter if it is available in time.

### 4.4 Kinematic determination of $Q^2$

Since the raw asymmetry has a linear dependence on  $Q^2$ , but a small dependence on other kinematic variables such as  $W$  or  $x$ , the largest systematic error in the physics asymmetry determination arises from the knowledge of the average  $Q^2$  of the events seen in each detector, weighted by detector response. The average  $Q^2$  will be determined from a detailed model of the spectrometer apertures and magnetic fields. The HRS spectrometers are very well understood from previous experiments, and preliminary studies indicate that we will be able to determine the average effective  $Q^2$  to better than 0.9%.

The uncertainty in beam energy  $E$  is  $<0.02\%$ , which contributes a negligible uncertainty to  $Q^2 = 4EE' \sin^2(\theta/2)$ . The HRS central momentum is known to  $<0.1\%$ , and the central angle can be determined to better than 1 mr. These generate an uncertainty in the central  $Q^2$  value of less than 0.9%, dominated by the uncertainty in the scattering angle. Previous experiments have determined the HRS angle to better than 0.5 mr, which would yield an uncertainty in  $Q^2$  of 0.5%.

## 4.5 Electromagnetic Radiative Corrections

Electromagnetic radiative corrections arise from the emission of photons by either the incident or scattered electron, either in the field of the nucleus (internal corrections), or in the field of another nucleus (external corrections). The ratio  $R_U$  of un-radiated to radiated spin-averaged cross sections is shown in Fig. 7 for the kinematics of the proposed measurements. At high  $W$  (low electron momentum  $P$ ), the radiated cross section is larger than the Born cross section, while the reverse is true at high  $W$ . In the kinematics of this proposal,  $R_U$  is mainly determined by the  $(x, Q^2)$  dependence of the spin-averaged structure function  $F_2$ . Of particular relevance is the ratio  $R_P$  of radiated to un-radiated  $ed$  parity-violating asymmetry. This ratio is close to unity for the kinematics of this proposal. The shape and magnitude of  $R_P$  is primarily determined by the probability for an electron to radiate a hard photon, and to a lesser extent by the  $(x, Q^2)$  dependence of  $F_2$  and  $A_p$ . We have estimated the systematic error in  $A_p$ ,  $A_d$ , and  $A_C$  to be about 0.5% over most of the kinematics of this experiment by considering the uncertainty in the unpolarized cross section (using several fits to world data) and in  $A_p$ , which will be largely determined by an iterative fit to the data of this proposal (although the elastic contributions to  $A_p$  are already reasonably well known from previous experiments). Uncertainties in the target dimensions and various materials which act as radiators have much smaller effects. These calculations were performed in the peaking approximation of Mo and Tsai [39]. Calculations with the more exact formulas of Ref. [40] are planned.

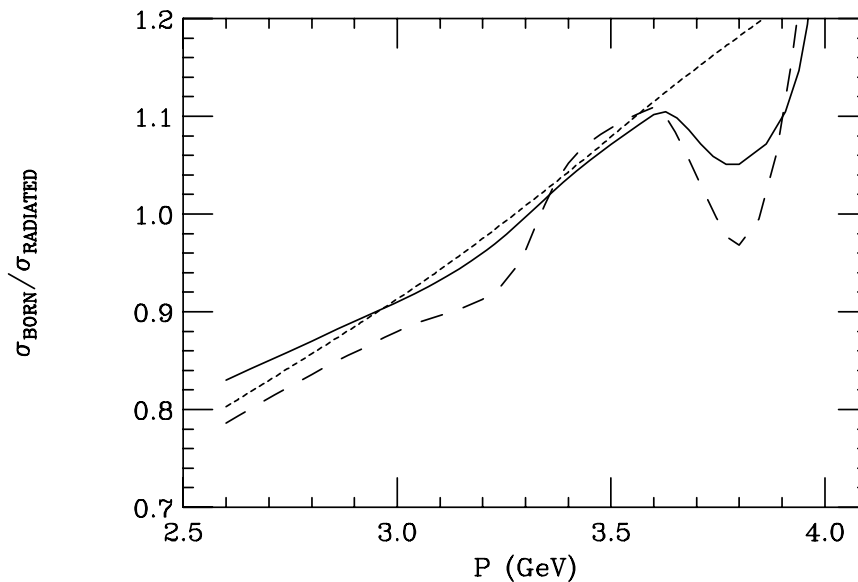


Figure 7: Radiative correction as a function of scattered electron momentum  $P$  for  $E = 4.8$  GeV. The curves are for deuterium (solid), proton (long dash), and carbon (short dashed).

## 4.6 Electroweak Radiative Corrections

Interpretation of the experimental results in terms of transition form factors (both axial and vector) requires the careful treatment of electroweak radiative corrections. In the case of the  $\Delta(1232)$  resonance, these can be sizable, and increase in relative importance as  $Q^2 \rightarrow 0$  [41]. We are not aware of calculations for higher mass resonances. For the interpretation of the data in terms of quark-hadron duality, and for simply searching for resonance structure in  $A_p$ , it is not crucial to have a complete understanding of electroweak radiative corrections, so we haven't included an uncertainty in the systematic error table. However one should keep in mind their importance in the interpretation of the data in terms of specific transition form factors.

## 4.7 Beam Asymmetries

Since the raw asymmetry in this experiment is 50 to 1000 times larger than other JLab PV experiments, our requirements on beam position, angle, energy, and charge asymmetries are relatively modest. Using the parity DAQ and the luminosity monitor as described in sections 3.3 and 3.5, we are confident that the false asymmetry due to beam quality will be under control, and the uncertainty will be negligible compared to the statistical uncertainty of the proposed measurement.

We will periodically reverse the half-wave plate at the injector to help cancel any residual false asymmetries.

## 4.8 Pion Contamination

The sign and magnitude of the pion asymmetry is of some physics interest in its own right, especially as it may impact backgrounds in experiments such as E158 and G0. It was seen to be small in the original SLAC experiment [1]. While we don't know of any calculations of the pion photoproduction asymmetry at our kinematics, the predicted asymmetry is of order  $10^{-7}$  at energies below 0.55 GeV [42], and  $1.3 \times 10^{-6}$  for excitation of the  $\Delta(1232)$  resonance [43]. These are both negligible compared to our expected electron asymmetry of about  $1 \times 10^{-4}$ .

The predicted  $\pi/e$  ratios shown in Table 1 are based on a fit to pion photoproduction data [44], which has proved to be accurate to 30% or better in past experiments. The  $\pi/e$  ratio is strongly  $W$ -dependent, approaching 1 in the highest  $W$  bin. We will measure both pions and electrons (see sections 3.7 and 3.8) during each run, yielding a measure of the pion asymmetry for each setting. The  $\pi/e$  ratio will be measured precisely using the regular HRS DAQ at low rates. Because the pion asymmetry is expected to be negligible compared to the electron asymmetry, only the dilution is expected to be important. With the proposed particle identification cuts, the pion contamination should be  $< 1\%$  to the electron sample (mainly due to pileup) for all kinematic conditions. Because we will have a good measure of the pion and electron rates, we can correct for this with a systematic uncertainty below 0.5%.

## 4.9 Pair Symmetric Background

In addition to the electron scattering events of interest, electrons can originate from decays of vector and pseudo-scalar mesons, and wide angle pair production. To a very good approximation, these processes are pair-symmetric, and can be measured with better than 3% accuracy by reversing the polarity of the spectrometers. Based on simulations with PYTHIA [45], we expect the largest source of pair-symmetric events to be from decays of photoproduced  $\pi^0$  mesons. The simulation is in reasonable agreement with data taken in Hall C over the past years. The highest predicted  $e^+/e^-$  ratio for this proposal is about 0.5% (at  $W = 2.1$  GeV), and drops rapidly at lower  $W$ . The asymmetry is expected to be very small, and this will be verified by taking data for a few hours with reversed spectrometer polarity. The net relative uncertainty on  $A_p$  and  $A_d$  will be  $< 0.2\%$ .

## 4.10 Target Related Systematics

Target boiling effects are expected to be very small for the proposed 25 cm LH2 and LD2 targets and  $85 \mu A$ . The increase in effective statistical fluctuations should be negligible, as described in section 3.4. In addition, the small-angle luminosity monitor will be used to verify a null asymmetry, as described in section 3.5, and provide additional confidence that target density fluctuations and helicity-correlated beam asymmetries are small.

With a magnetic field at the target of  $< 10$  Gauss, the proton polarization will be less than 0.001%, leading to a negligible double-spin asymmetry from the  $g_1$  structure function.

Impurities in the liquid hydrogen are typically less than 0.1%, and are expected to cause a negligible effect on  $A_p$  since the asymmetry has only a weak dependence on atomic number  $A$ . The largest effect will be from the aluminum endcaps, for which the asymmetry is typically 20% larger than for the proton is the DIS limit. Since the endcaps contribute only a few percent of the count rate, this correction is small, and will be constrained by the carbon asymmetry measurements, for which the asymmetry should be nearly identical to aluminum (after making a small neutron excess correction based on the proton and deuteron measurements). For the deuteron measurements, the biggest correction comes from the fraction of hydrogen. This will be measured to better than 0.2%, leading to a negligible systematic error on  $A_d$ .

## 5 Request

We request 14 days of production data and one day for checkout, beam polarization measurements, and configuration changes, as summarized in Table 3. While 4.8 GeV is optimal, energies between 4.6 and 5.2 GeV would be acceptable, yielding slightly reduced statistics at the lower energy and introducing a slight gap in the  $W$  coverage at increased energies.

Table 3: Beam time request. All data taken with 4.8 GeV beam and both HRS spectrometers at  $12.5^\circ$ .

Target	$P$ (HRS-L)	$P$ (HRS-R)	time
LH2	4.0 GeV	3.2 GeV	72 hours
LH2	3.6 GeV	2.8 GeV	72 hours
LD2	4.0 GeV	3.2 GeV	48 hours
LD2	3.6 GeV	2.8 GeV	48 hours
Carbon	4.0 GeV	3.2 GeV	48 hours
Carbon	3.6 GeV	2.8 GeV	48 hours
Pass Change			8 hours
Polarimetry runs			8 hours
$e^+$ Asymmetry			8 hours
Total			360 hours (15 days)

This experiment requires only standard Hall A equipment, with the exception of the upgraded Compton polarimeter and the high speed DAQ system which are being built for the DIS-parity measurement (E05-007). We will work with the E05-007 collaboration on the implementation of the necessary equipment.

Figure 8 shows the projected uncertainties for the asymmetries for each target.

## 6 Physics Summary

The physics results will be the first ever measurements of the PV asymmetry in inelastic electron scattering from the proton and deuteron in the resonance region beyond the  $\Delta(1232)$ . The precision will be sufficient to observe resonance structure at the 5% level, and to test local and global duality at the few percent level, comparable to the level at which duality is observed in the unpolarized structure functions. The PV asymmetry is also useful because it is more sensitive to the down and strange quarks than the unpolarized structure functions, allowing us to study the d/u ratio in the proton without the nuclear corrections that enter when studying the neutron in nuclear targets.

Data on deuterium and carbon will allow us to look for nuclear dependence in the PV asymmetry. Recent measurements of the nuclear dependence of  $F_2$  in the resonance region show nearly identical effects to the EMC measurements in the DIS limit [14], while recent calculations show that medium modifications may be very different in spin-averaged and spin-dependent structure functions, with a significant dependence on quark flavor [15].

The results will not only be interesting in their own right as a new way to probe the fundamental structure functions of the proton and neutron, but will be of great value in the growing world-wide program of neutrino studies. The new data will also provide details about the backgrounds in other PV experiments, and are needed as input to

## 7 Collaboration

The collaboration has many members with recent experimental experience in precision electron PV experiments (such as SLAC E158 and JLab HAPPEX), and we are confident that we will be able to control systematic errors at the few percent level. The collaboration has large overlap with the DIS-parity collaboration that is working on the upgrades to the Compton polarimeter and the fast data acquisition system.

## References

- [1] C.Y. Prescott *et al.*, Phys. Lett. 77B, 347 (1978); 84B, 524 (1979).
- [2] NuTeV Collaboration, G.P. Zeller *et al.*, Phys. Rev. Lett. 88 (2002) 091802. Minor revisions in hep-ex/0110059 v.3 (2003) and hep-ex/0203004 v.3 (2003).
- [3] Particle Data Group, Phys. Rev. D 66, (2002) 010001.
- [4] SLAC E158 Collaboration, P.L. Anthony *et al.*, Phys. Rev. Lett. 92, 181602 (2004); hep-ex/0504049.
- [5] A. D. Rujula, H. Georgi and H. D. Politzer, Ann. Phys. 103, 315 (1977).
- [6] E. D. Bloom and F. J. Gilman, Phys. Rev. Lett. 25, 1140 (1970).
- [7] I. Niculescu *et al.*, Phys. Rev. Lett. 85, 1186 (2000).
- [8] C. E. Carlson, N. C. Mukhopadhyay, Phys. Rev. Lett. 74, 1288 (1995).
- [9] W. Melnitchouk, R. Ent, C. E. Keppel, Phys. Rept. 406:127-302 (2005).
- [10] D.A. Harris *et al.*, hep-ph/0410005 (2004); A. Bodek, I. Park, and Un-ki Yang, hep-ph/0411202 (2004).
- [11] E.A. Paschos, M. Sakuda, I. Schienbein, J.Y. Yu, hep-ph/0408185 (2004); E.A. Paschos, J.Y. Yu, M. Sakuda, hep-ph/0308130 (2003); E.A. Paschos, J.Y. Yu, hep-ph/0107261 (2001); S. Kretzer and M. H. Reno, hep-ph/0208187 (2002).
- [12] R. Belusevic and D. Rein, Phys. Rev. D38, 2753 (1988); C. Carlson and N. Mukhopadhyay, Phys. D47, 1737 (1993).
- [13] M. Hirai, S. Kumano, and M. Miyama, Phys. Rev. C70, 044905 (2004); M. Hirai, S. Kumano, and M. Miyama, Phys. Rev. D64, 034003 (2001)
- [14] J. Arrington, R. Ent, C.E. Keppel, J. Mammei, I. Niculescu, nucl-ex/0307012.

- [15] I.C. Cloet, W. Bentz, and A.W. Thomas, nucl-th/0504019.
- [16] Jason R. Smith and Gerald A. Miller, nucl-th/0505048.
- [17] J.E. Amaro, M.B. Barbaro, J.A. Caballero, T.W. Donnelly, A. Molinari, Physics Reports 368, 317 (2002); M.B. Barbaro, J.A. Caballero, T.W. Donnelly, A. Molinari, Phys. Rev. C69, 035502 (2004); A. De Pace, M. Nardi, W.M. Alberico, T.W. Donnelly, A. Molinari, Nucl. Phys. A741, 249 (2004).
- [18] M.J. Musolf *et al.*, Phys. Rept. 239, 1 (1994).
- [19] S.L. Adler, Ann. Phys. 50 (1968) 189.
- [20] R. Cahn and F. Gilman, Phys. Rev. D17, 1313 (1978).
- [21] D.R.T. Jones and S.T. Peteov, Phys. Lett. B91 (1980) 137; L.M. Nath, K. Schilcher, M. Kretschmar, Phys. Rev. D 25 (1982) 2300.
- [22] G. F. Sacco, Ph.D. Thesis, University of Connecticut, 2004 (unpublished).
- [23] J. Blumlein *et al.*, HERA Workshop Vol. 1, p. 69, Hamburg 1989.
- [24] J. Erler and P. Langacker, Particle Data Group, Phys. Rev. D 66, 010001 (2002).
- [25] S. Kuhn, private communication.
- [26] F. Close and N. Isgur, Phys. Lett. B509, 81, (2001).
- [27] J. Alcorn *et al.*, Nucl. Instrum. Meth. A **522**, 294 (2004).
- [28] R. Michaels *et al.*, JLab E03-001, Neutron skin of  $^{208}\text{Pb}$  Through Parity Violating Electron Scattering, *A* rating. URL: <http://www.jlab.org/~rom/pbupdate.ps>
- [29] R. Michaels, P.E. Reimer and X. Zheng, JLab E05-007,  $\vec{e}^-^2\text{H}$  Parity Violating Deep Inelastic Scattering at CEBAF 6 GeV, *A*<sup>-</sup> rating. URL: <http://hallaweb.jlab.org/experiment/E05-007/>
- [30] HAPPEX-I archival paper, K.A. Aniol *et al.*, Phys. Rev. C 69, 065501 (2004).
- [31] D.S. Armstrong, presentation at the Feb. 18, 2005 HAPPEX collaboration meeting: [hallaweb.jlab.org/experiment/HAPPEX/minutes/05Feb18/DSA\\_boil.pdf](http://hallaweb.jlab.org/experiment/HAPPEX/minutes/05Feb18/DSA_boil.pdf)
- [32] H. Ibrahim, P. Ulmer, N. Liyanage, Hall A Technical Note JLAB-TN-02-032, (2002).
- [33] R. Michaels, presentation at the Feb. 18, 2005 HAPPEX collaboration meeting: [hallaweb.jlab.org/experiment/HAPPEX/minutes/05Feb18/Happex\\_Bob\\_19feb05.pdf](http://hallaweb.jlab.org/experiment/HAPPEX/minutes/05Feb18/Happex_Bob_19feb05.pdf)
- [34] P. Souder, HAPPEX technical note.

- [35] X. Zheng, “*JLAB Hall A detector PID efficiency analysis using high electron and high pion rate data*”: <http://hallaweb.jlab.org/physics/experiments/he3/A1n/>
- [36] D. von Harrach, F.E. Maas *et al.*; <http://www.kph.uni-mainz.de/A4/>
- [37] S. Koebis, P. Achenbach, *et al.*, Nucl. Phys. B (Proc. Suppl.) **61B**, 625 (1998).
- [38] G. Batigne, *et al.*, “Deadtime Corrections for the French Electronics”, G0 Internal Memo.
- [39] Y.S. Tsai, Report No. SLAC-PUB-848, 1971; Rev. Mod. Phys. 46 (1974) 815.
- [40] D.Y. Bardin *et al.*, Yad. Phys. 29 (1979) 499; Nucl. Phys. B 197 (1982) 1.
- [41] Shi-Lin Zhu, C.M. Maekawa, G. Sacco, B. R. Holstein,, M.J. Ramsey-Musolf, Phys. Rev. D65 (2002) 033001.
- [42] S-P. Li, E.M. Henley and W-Y.P. Hwang, Annals of Physics 143 (1982).
- [43] S.L. Zhu, C.M. Maekawa, B.R. Holstein and M.J. Ramsey-Musolf, Phys. Rev. Lett. 87 (2001) 201802.
- [44] D.E. Wiser, Ph.D thesis, U. Wisconsin, 1977 (unpublished).
- [45] T. Sjostrand, Computer Physics Commun. 82, 74 (1994).

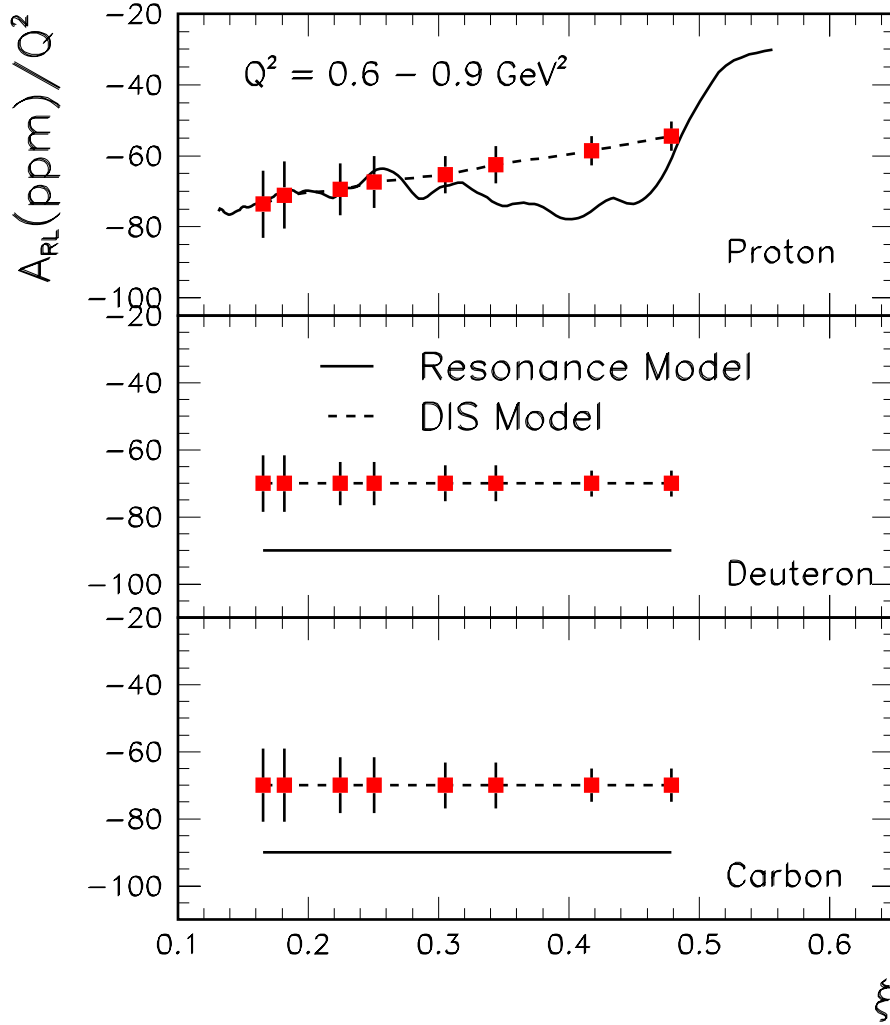


Figure 8: Expected asymmetry divided by  $Q^2$  (in ppm/GeV<sup>2</sup>) for the DIS and simplified (pure  $I = 1$  transition) resonance region models) as a function of  $\xi$  along with projected errors for the proposed measurements on the three targets. Each spectrometer setting has been divided into two  $W$  bins. The error bars shown include both statistical and systematic ( $<2\%$ ) uncertainties.